First-principles study of two-dimensional electron gas on a layered Gd_2C electride surface

Jinwoong Chae,[1] Junsu Lee,[1] Youngtek Oh,[2] and Gunn Kim[3,*]

[1]*Department of Physics and HMC, Sejong University, Seoul 05006, Republic of Korea*

[2]*Samsung Advanced Institute of Technology, Suwon 16678, Republic of Korea*

[3]*Department of Physics & Astronomy and HMC, Sejong University, Seoul 05006, Republic of Korea*

(Received 30 June 2021; revised 19 August 2021; accepted 19 August 2021; published 2 September 2021)

Electrides are ionic compounds in which electrons behave as anions in the interior of a positively charged framework. As a layered electride, Gd_2C receives attention because of its ferromagnetism. Although previous research has focused on the bulk properties of Gd_2C, few studies have focused on ultrathin layers or surfaces for two-dimensional (2D) characteristics. Here, we report a first-principles study of the electronic properties of few-layer Gd_2C structures. Gd_2C has a work function of 3.35 eV. When a layered electride is exfoliated, the interstitial layer becomes a surface and may be exposed to the outside. Because the interlayer region has changed to the surface, the properties of the electron gases once located in the interlayer in the past will also change. We found that the surface anionic electrons accounted for about 25% of the number of electrons in the interlayer region in the absence of an external electric field. When we applied an external electric field, the number of surface electrons increased, and the increase was proportional to the square of the field intensity. Since the electronic properties of 2D materials can be understood through scanning tunneling spectroscopy (STS), we also performed the STS simulations. At −0.9 eV, the STS image was blurred because of surface anionic electrons. In contrast to the spin-up electron, an interlayer band of the spin-down electron crossed the Fermi level in the ultrathin Gd_2C layers. Our findings open a possibility that the spin-polarized electronic gas in the few-layer electride could be used for spintronics.

DOI: 10.1103/PhysRevB.104.125403

I. INTRODUCTION

In electrides, interstitial anionic electrons (IAEs) are confined in the cavities of a positively charged framework [1,2]. Electrides have attracted attention because of their exotic properties such as a low work function and charge transfer characteristics caused by anionic electrons [3–9]. Numerous types of solid electride salts have been synthesized; however, most are unstable at room temperature or under humid atmospheres. Therefore, the development of stable electrides in any environment is a critical challenge. The first thermally and chemically stable electride in air was $Ca_{24}Al_{28}O_{64}$, which shows various characteristics, such as metal-insulator transition, metal-semiconductor transition, and superconductor transition [10–14]. Electrides can be applied to electron emitters [15] and catalysts [16].

Interestingly, a layered structure of dicalcium nitride, Ca_2N, was synthesized [6], called two-dimensional (2D) electride. In the 2D electride, a delocalized anionic electron gas exists in the interlayer space of the layered electride. Therefore, the positively charged Ca_2N layers are separated by electron gas layers. Since then, Y_2C [17] and Gd_2C [18], which are representative carbide electrides, have also been successfully synthesized. 2D electrides exhibit numerous unique properties, such as magnetoresistance, low work functions, and anisotropy of resistance. Because the materials are also layered structures, the resistance is very small on the same plane; however, the resistance to current flowing in a direction perpendicular to the plane is relatively large. The 2D electrides exhibit different characteristics depending on the distribution of the anionic electrons [6,7,17,19]. When distributed anionic electrons are delocalized, as in Ca_2N, the anionic electrons behave like free electrons with high mobility [6]. In contrast, when the anionic electrons are strongly localized, as in Y_2C, the anionic electrons show low mobility [7,17,19]. The anionic electrons in Gd_2C have a partially delocalized distribution, which implies that the anionic electrons behave like free electrons with considerable mobility and exhibit strong spin magnetic moments [18,20,21].

Experimental physics studies have focused on the bulk characteristics of layered electrides because the surface electronic structure of 2D electrides is chemically unstable because of the highly reactive anionic electrons. In addition, few theoretical studies have focused on surfaces or two-layered structures [22]. One way to apply the exotic properties of electrides is to form ultrathin sheets, thus exposing the electron gas layer residing near the surface. Like graphene obtained from graphite [23], ultrathin electrides can be fabricated using the exfoliation method [24]. In 2018, Oh *et al.* exfoliated the Y_2C electride under ultrahigh vacuum conditions to study the atomic and electronic structure of its surface using scanning tunneling microscopy (STM) and scanning tunneling spectroscopy (STS) [25]. They revealed that anionic electrons absorbed into the Y_2C top layer were resurged onto the surface when an electric field is applied. When vertical

*Corresponding author: gunnkim@sejong.ac.kr

heterostructures were fabricated with a 2D electride and transition metal dichalcogenide (TMDC), the TMDC structure changed because of charge transfer [26]. To understand the physical properties of the interface or molecular adsorption formed by contacting other materials, one must know the surface properties of the electrides. In addition, as has been observed for graphene and TMDC [27,28], few-layer structures have slightly different properties from bulk structures in terms of atomic and electronic properties.

The Gd_2C electride is a ferromagnetic material, and the partially delocalized electron gas in the interlayer space also possesses spin magnetic moments [18]. To use Gd_2C as a spin device, it must be in contact with other materials. Thus, the various interesting electronic and magnetic properties of the Gd_2C surface must be understood. In this paper, we report a first-principles study of the electronic properties of few-layer Gd_2C structures ($N = 2$, 3, 4, and 5) compared with the monolayer and the bulk structure. We provide the optimized structures, electronic band structures, density of states (DOS), total charge density differences, and work functions for the cases to describe the few-layer Gd_2C. In addition, we confirm the charges, which exist above the surface, by investigating the electric field effects. Our study focuses on the surface properties of IAEs. We also present simulated STS and STM images.

II. COMPUTATIONAL METHOD

We investigated the electronic and magnetic properties of bulk and freestanding few-layer Gd_2C structures by first-principles calculations based on spin-polarized density functional theory (DFT). In the computations, we used the Vienna *ab initio* simulation package (VASP) [29,30]. A plane-wave basis set was used to describe the electronic charge density. The interactions between the electrons and ions were described using the projector-augmented-wave (PAW) method [31,32]. The exchange-correlation energy was modeled using the Perdew-Burke-Ernzerhof (PBE) type generalized gradient approximation (GGA) functional [33]. The kinetic energy cutoff was set at 600 eV, and a Γ-centered $10 \times 10 \times 1$ k-point grid was used for the electronic structure calculations. The convergence tolerance was set at an energy of 10^{-6} eV.

We considered the onsite Coulomb interaction in Gd $4f$ orbitals for the GGA + U calculation without including spin-orbit coupling [34–36]. We chose the Hubbard parameter $U = 6.7$ eV and exchange interaction parameter $J = 0.7$ eV. Therefore, the effective U value ($U_{\text{eff}} = U - J$) was 6 eV, which is the same as that used in previous reports [37,38]. We used Grimme's DFT-D3 method for van der Waals corrections [39]. A uniform electric field of 0.1 V/Å was applied to the few-layer systems, which was normal to the surface plane. The VESTA and Gnuplot packages were employed to visualize the model structures and plot the band structures and DOSs.

III. RESULT AND DISCUSSION

A. Optimized structure, formation energy, and work function

First, we obtained optimized structures of bulk and few-layer Gd_2C structures (Fig. 1). For the bulk structure, the lattice parameter a was 3.606 Å and $c/a = 5.144$. The Gd-C bond length was 2.48 Å, and the interlayer distance was 3.36 Å, which agrees well with the data from a previous *ab initio* study [38]. When a surface appears due to exfoliation and a layer in contact with a vacuum is created, symmetry is broken, resulting in structural changes. Consequently, as shown in Fig. 1, in the top layer in contact with the vacuum, Δz between the upper Gd atom and the carbon atom is 1.31 Å, and Δz between the lower Gd atom and the carbon atom is 1.39 Å. In contrast, in the inner layers, Δz between the Gd atom and the carbon atom, like the bulk, is nearly uniform at 1.35 Å. Furthermore, as shown in Figs. 1(e) and 1(f), the interlayer distance is shorter in the deeper interior than in the outermost interior. Therefore, we expect that the electronic

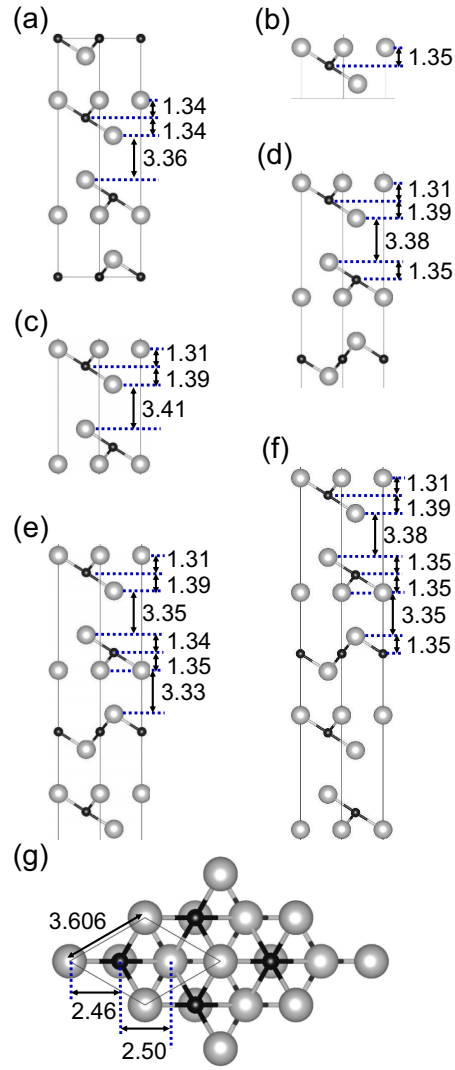

FIG. 1. Optimized structure of few-layered Gd_2C. In this figure, gray color indicates the Gd atom, and black is the carbon atom. (a) ABC-stacked bulk, (b) monolayer ($N = 1$), (c) bilayer ($N = 2$), (d) trilayer ($N = 3$), (e) tetralayer ($N = 4$), and (f) pentalayer ($N = 5$) of Gd_2C. (g) Top view of the Gd_2C bilayer (2×2 supercell). N represents the number of layers. The numbers denote the distances (Δz) in the z direction in the unit of Å. In (g), the numbers represent the distance in the lateral direction (xy directions) in the unit of Å.

TABLE I. Formation energies and work functions of few-layered Gd_2C structures. The energy is in the unit of eV.

Number of layers	Formation energy	Work function
$N = 1$	1.224	3.426
$N = 2$	1.210	3.374
$N = 3$	1.210	3.351
$N = 4$	1.200	3.351
$N = 5$	1.189	3.350

properties are different from those of the bulk near the surface due to the breakage of symmetry. We will explain this phenomenon in detail later.

The formation energy of each structure was then calculated. The formation energy (E_{form}) can be defined as follows:

$$E_{\text{form}} = E_{\text{few-layer } Gd_2C} - n_{\text{atom}} \cdot E_{\text{bulk}}, \quad (1)$$

where $E_{\text{few-layer } Gd_2C}$ is the total energy of the system, E_{bulk} is the total energy of bulk Gd_2C per atom, and n_{atom} is the number of atoms in a unit cell of a few-layer structure. The formation energies are presented in Table I. As the number of layers increases, the formation energy decreases, which means that structures with a larger number of layers are energetically preferred.

We then studied the layer dependence of the work function of the few-layer Gd_2C structures. Local potential profiles along the z direction were obtained. The work function ϕ was calculated as follows:

$$\phi = E_v - E_F, \quad (2)$$

where E_v is the vacuum level and E_F the Fermi level. As the number of layers increases, the work function approaches 3.35 eV, almost identical in the trilayer to the pentalayer. As listed in Table I, the monolayer has a work function that is ∼0.07 eV larger than that of the others. Another famous layered electride, Y_2C, also shows the same layer dependence of the work function [25]. The Gd_2C pentalayer has a smaller work function by 0.40 eV than the Y_2C pentalayer (3.75 eV) [25]. According to a recent STM study, the Y_2C surface has the work function of 3.51 eV [25]. Therefore, we predict that the value of the clean $Gd_2C\,(0001)_H$ surface could be about 3.1 eV in the experiment. If the surface is not clean, the work function would be slightly greater or less than 3.1 eV.

B. Electronic structure

Next, we investigated the electronic properties of layered Gd_2C. Previous studies on electrides having a stacked structure have not dealt with the relationship between the energy dispersions patterns or energy positions of bands corresponding to the IAE state with the number of layers. In particular, the IAE states that are in the conduction band have not been studied. In the present study, we focus on the energy bands created by these IAE states by calculating the electronic structure of few-layer Gd_2C structures. They are all metallic and ferromagnetic and are independent of the number of layers. A gadolinium atom has seven unpaired f electrons [40]. The atomic spin magnetic moment of each Gd atom in Gd_2C is

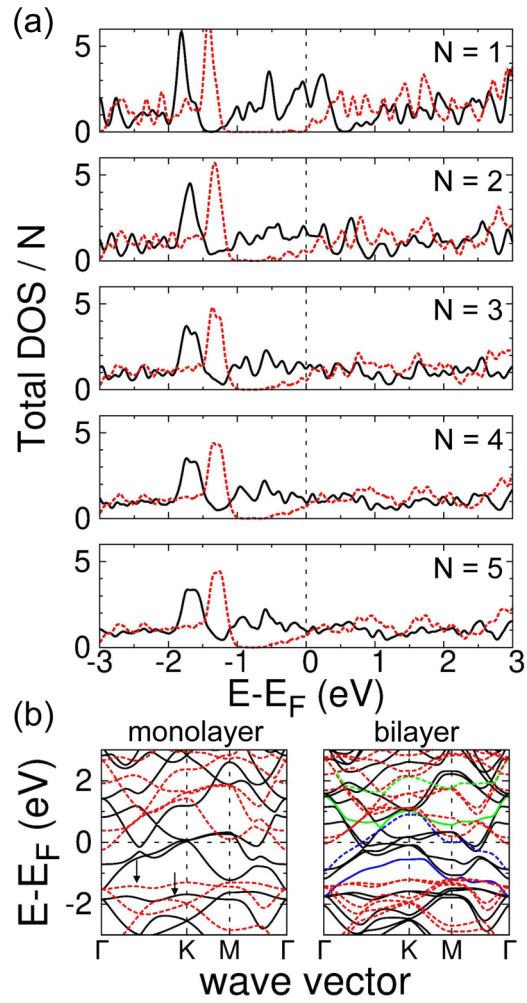

FIG. 2. (a) DOS plots and (b) electronic band structures of few-layer Gd_2C systems. Solid (dotted) lines indicate the electronic bands of the spin-up (spin-down) electrons. The blue and green lines denote the bands of IAE states. For comparison, the DOS was divided by N, i.e., the number of layers.

≈7.3 μ_B, which agrees well with previous reports on bulk Gd_2C [18,20,41,42].

Figure 2(a) shows the DOS plots of the Gd_2C models. For both spins (up and down), the highest DOS peaks between −2 and −1 eV in all structures were not related to IAEs because the monolayer, which does not have the IAE states, also had peaks in the same range. When the number of layers increases, the peaks become smaller and more broadened owing to the interlayer interaction. The highest DOS peaks originate from the hybridization of C $2p$ and Gd $5d$ orbitals, and they are localized states corresponding to almost flat bands. In Fig. 2(b), the two bands in the monolayer, indicated by arrows, are nearly flat along the path from Γ to M.

In the valence band of the bilayer, there is a band (a solid blue line) between −1.5 and −0.5 eV for the spin-up state. A band (a dotted blue line) crosses the Fermi level for the spin-down state in the range of −1.0 to +1.0 eV. The bands were not observed in the monolayer. The bands indicated by green lines were also not observed in the monolayer but appeared in the conduction band of the bilayer. The blue and green lines

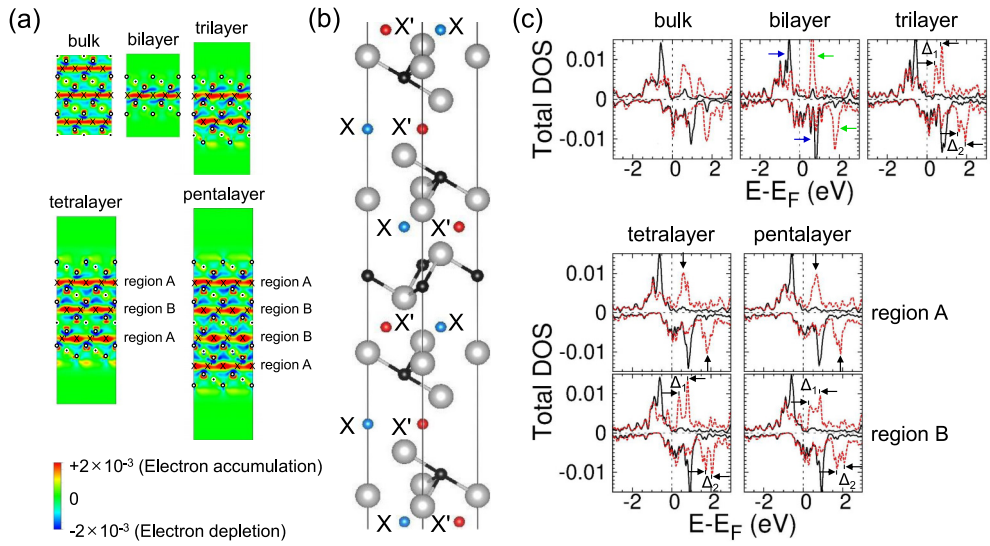

FIG. 3. (a) Total charge density difference plots of few-layered Gd_2C. (b) Ball-and-stick models show the X and X′ sites in the bulk. (c) DOS plots of X and X′ sites. In the DOS plots, the X and X′ sites are denoted by solid and dotted lines, respectively.

correspond to the states of the electrons gathered in the interstitial space. In particular, the spin-down band passing through the Fermi level is expected to play an essential role in spin transport. As mentioned earlier, this band originates from an IAE state, which may be likened to strawberry jam spread between two pieces of bread, and thus, the state will be preserved even though molecules are adsorbed on the outer surface of Gd_2C. Thus, we expect electrons in the spin-down state to be conducted well through this channel. We also provide the Fermi velocities of the monolayer to the pentalayer for the spin-down bands crossing the Fermi level in Table V, indicated by circles in Fig. 6 of Appendix A. The IAE states for all cases ($N = 2$, 3, 4, and 5) were in a similar energy range.

Figure 3(a) shows plots of the total charge density differences of the models. We found that electrons accumulated in the interlayer region and depleted in the Gd_2C layers. In contrast, electrons were not accumulated or depleted at the surface of the top layer. To understand the density distribution of electrons in the interlayer region and their electronic properties, we selected two sites in the same interlayer space and calculated the spin-polarized DOS of the two sites. The two sites are labeled X and X′, as shown in Fig. 3(b). To calculate the DOS of the X and X′ sites, we assumed that fictitious atoms were placed at X and X′ and calculated the DOS of those fictitious atoms by considering spheres with a radius of 0.4 Å.

As shown in Fig. 3(c), the DOS plots for the X and X′ sites are different. High peaks occur between −1 and 2 eV. For the Gd_2C bilayer, the high DOS peaks indicated by the blue and green arrows are the IAE states corresponding to the blue and green lines in Fig. 2(b), respectively. As described above, the interlayer distance is not uniform within the thin layer, unlike in the bulk (see Fig. 1). Therefore, we distinguish region A from region B for the interlayer space, as shown in Fig. 3(a). As shown in Fig. 1, region A has a larger spacing than region B.

For the spin-up electrons, we observed that the DOS peak at X′ between 0 and 1 eV shows different energy splits in regions A and B for the $N = 4$ and $N = 5$ cases [see Fig. 3(c)]. Meanwhile, for spin-down electrons, the DOS peaks of X′ between 1.5 and 2.5 eV exhibit the same phenomenon. This phenomenon occurs when the interaction between the IAE states in different interlayer regions acts as a perturbation and breaks the energy degeneracy. This phenomenon is prominent in the conduction band. The interpeak gap appears larger in region B than in region A because region B is slightly narrower. Energy splitting was prominent in region B. We labeled the energy spacings Δ_1 for the spin-up state and Δ_2 for the spin-down state, and the values are summarized in Table II. We found that Δ_1 was greater than Δ_2 for both $N = 4$ and $N = 5$. Region A showed wide spacing, and the IAEs here do not have IAEs on the vacuum side. Consequently, little interaction was observed with this vacuum side, and the interpeak spacing was small in region A.

C. Electronic density 2 Å above the surface

In the bulk structure, because positively charged Gd_2C layers are stacked repeatedly, electrons can gather between the layers. However, when the symmetry is broken and the surface is exposed, there are no more positively charged layers above the surface. Thus, no electron layer was formed on the surface. What happens if a bias voltage is applied to the surface? Will the electrons absorbed in the top layer return to the surface? To determine the effects of the electric field, we calculated the electronic structures of the mono-, bi-, and trilayer systems in

TABLE II. Δ_1 and Δ_2 for the interpeak spacing corresponding to the spin-up and spin-down states, respectively. Δ_1 and Δ_2 have the unit of eV.

Number of layers	Δ_1	Δ_2
$N = 3$	0.294	0.320
$N = 4$	0.427	0.307
$N = 5$	0.481	0.374

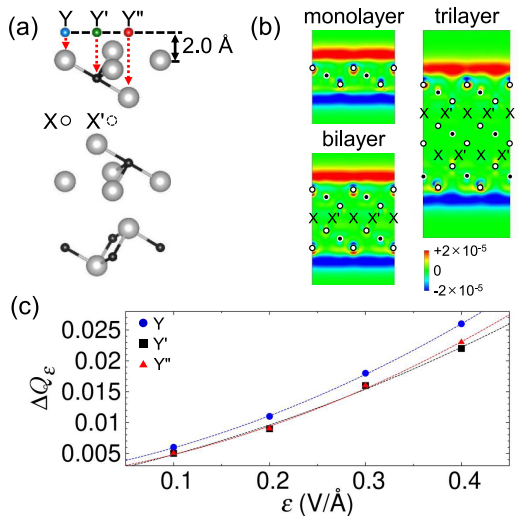

FIG. 4. Resurgence of the anionic electrons at the surface by the electric field effect. (a) Spatial positions of the Y, Y′, Y″, X, and X′ sites. (b) Electronic density difference plot for the mono-, bi-, and trilayer structures under the electric field of 0.1 V/Å. (c) The calculated number ($\Delta Q_{\mathcal{E}}$) of electrons pulled out by the electric field $\mathcal{E}$ in the bilayer. The fitted lines show the quadratic behavior.

the presence of a uniform electric field of 0.1 V/Å, which has a similar field strength as that produced by the sharp STM tip [43,44].

We chose three sites 2 Å above the surface Gd atom, labeled Y, Y′, and Y″, in Fig. 4(a). We note that fictitious atoms are located at the Y, Y′, and Y″ sites with a radius of 0.4 Å, which is the same as at the X and X′ sites. We were able to reveal the difference in the density between the three sites and Gd atoms with and without an electric field. Even though the electronic density difference [= ρ(with electric field) − ρ(without electric field)] is small, a small amount of charge is pulled out at the surface by the electric field, as shown in Fig. 4(b). Because of charge screening, the electric field effect was confirmed only at the surface but was not observed at the interstitial regions.

To obtain further information on the electric field effect, we first calculated the number of electrons at the Y, Y′, Y″, X, and X′ sites in the bilayer. The number of electrons (N_{site}) can be defined as follows:

$$N_{\text{site}} \equiv \int_{-\infty}^{E_F} \{D^{\text{up}} + D^{\text{down}}\} dE, \tag{3}$$

where D^{up} and D^{down} represent the DOSs of the spin-up and spin-down states, respectively. We obtained the ratio ($\eta_{y/x}$) of the Y (Y′, Y″) site to the X (X′) site by calculating the number of electrons as follows:

$$\eta_{y/x} = \frac{N_y}{N_x}, \tag{4}$$

where subscript x (y) corresponds to X or X′ (Y, Y′ or Y″). We present the results for $\eta_{y/x}$ in Table III. In the absence of an external electric field, the number of electrons at the Y, Y′, or Y″ site is 25-27% compared to the number of electrons at the X or X′ site. This result implies that few charges remain at 2 Å above the surface. Therefore, we concluded that the charges are surface anionic electrons (SAEs). Our Mulliken charge analysis shows that the upper Gd atoms at the top layer has 0.04 e more than other Gd atoms in the other layers.

TABLE III. The ratio ($\eta_{y/x}$) of the Y (Y′, Y″) site to the X (X′) site obtained by calculating the number of electrons.

Site	X	X′
Y	0.268	0.256
Y′	0.269	0.256
Y″	0.266	0.254

Now, we consider the number of the electrons resurging at the same site by applying an electric field. We calculated the difference in the number of electrons before and after applying the electric field effect ($\Delta Q_{\mathcal{E}}$), which can be defined as follows:

$$\Delta Q_{\mathcal{E}} = N_{\mathcal{E}} - N_0, \tag{5}$$

where $N_{\mathcal{E}}$ is the total number of electrons in the presence of the electric field and $\mathcal{E}$ is the electric field strength (0.1, 0.2, 0.3, or 0.4 V/Å). N_0 is the total number of electrons in the absence of an electric field. The $\Delta Q_{\mathcal{E}}$ values is listed in Table IV. As the strength of the electric field increases, the number of electrons in the SAE sites increases. In contrast, the number of electrons at the site in the interlayer region hardly changes because the Gd_2C layer is a good metal and screens the electric field.

How many electrons leave the surface when an electric field is applied? When 0.1 V/Å (0.4 V/Å) is applied, 0.005 e (0.026 e) emerge from the Gd_2C surface. As shown in Fig. 4(c), $\Delta Q_{\mathcal{E}}$ is proportional to $\mathcal{E}^2$, which can be explained by the perturbation theory for charge density. Notably, $\Delta Q_{\mathcal{E}}$ on the Y site increases rapidly, whereas the $\Delta Q_{\mathcal{E}}$ values of Y′ and Y″ sites are not significantly affected by the electric field. This result implies that the charge on the site is related to the atomic orbital of the Gd atom at the surface, which will be discussed later.

Finally, we investigated the surface properties of Gd_2C layers. First, we calculated the DOS of the SAE sites for the mono-, bi-, and trilayer [Fig. 5(a)]. Significantly, if we compare the DOS of the monolayer and bilayer (or trilayer), we can see more prominent peaks at −0.9, −0.4, +0.7, and +0.8 eV in the DOS of the bilayer. However, the DOS peaks of the monolayer at these energies are not very clear. The peak at +0.7 eV is clearly visible in the bilayer, which is not visible in the monolayer. This peak is not conspicuous in the trilayer

TABLE IV. The total number of electrons on sites without applying an electric field, and the difference in the effect of the number of electrons before and after applying the electric field on the bilayer.

Site	N_0	$\Delta Q_{0.1}$	$\Delta Q_{0.2}$	$\Delta Q_{0.3}$	$\Delta Q_{0.4}$
X	1.421	0.000	0.000	0.000	0.003
X′	1.489	0.000	0.000	0.000	0.005
Y	0.381	0.006	0.011	0.018	0.026
Y′	0.382	0.005	0.009	0.016	0.022
Y″	0.378	0.005	0.009	0.016	0.023

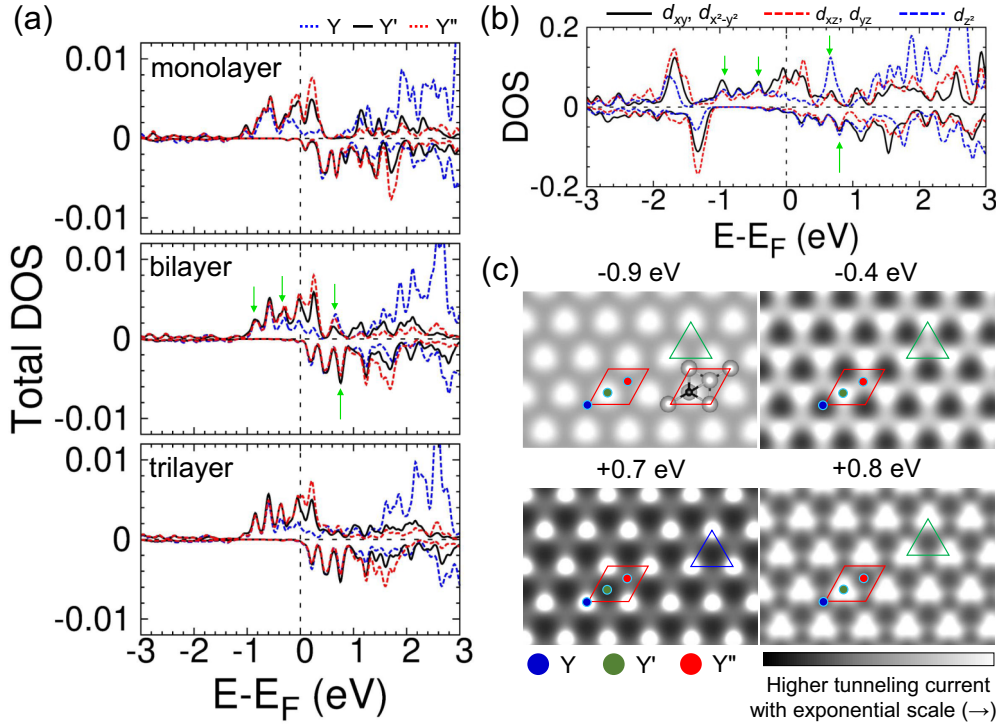

FIG. 5. The atomic DOS and STS simulation results on the surface of Gd_2C. (a) The atomic DOS of the Y, Y′, and Y″ sites for the mono-, bi-, and trilayer systems and (b) the orbital decomposed DOS of the Gd atom at the bilayer surface. In (a), the blue (black, red) line indicates the Y (Y′, Y″) site. In (b), the black (red, blue) line indicates the d_{xy} and $d_{x^2-y^2}$ (d_{xz} and d_{yz}, d_{z^2}) orbitals of the Gd atom. (c) Simulated STS images of the bilayer Gd_2C surface. The images were obtained under the constant-height (2 Å) mode from the computational simulations. The rhombus shape in red color represents the unit cell of Gd_2C.

because it is divided into two smaller peaks due to energy splitting. The above four peaks also appear in the DOS of the X and X′ sites, as shown in Fig. 3(c). In the DOS plots, the peaks near −0.9, −0.4, and +0.8 eV are dominant at X, and the DOS peak near +0.7 eV is dominant at X′.

When the surface is exposed, the X site of the bulk corresponds to the Y″ site in a few layers because Gd_2C has an ABC-stacked structure. Therefore, the surface is revealed, and part of the IAE of the X site may remain at the Y″ site. The remaining IAE is absorbed by the Gd atom in the top layer. For the trilayer, the positions of the significant DOS peaks of X match those of Y″. The DOS peaks of Y″ slightly shift upwards for the bilayer because of small charge transfer.

We also compared the d orbital contributions of the Gd atoms to the DOS of the SAE sites. The projected DOS of the surface Gd atom at the top layer decomposed to the d orbitals, as shown in Fig. 5(b). We found that the d_{xy} and $d_{x^2-y^2}$ orbitals exhibit energy degeneracy, and the d_{xz} and d_{yz} orbitals also exhibit degeneracy. Figures 5(a) and 5(b) show that the d orbitals of the Gd atom affect the prominent DOS peaks (indicated by arrows) of the bilayer. Near the Fermi level, the Y′ and Y″ sites are influenced by the d_{xz} and d_{yz} orbitals of the Gd atom, whereas the Y site is influenced by the d_{z^2} orbital. In particular, the DOS peaks of the Y site are dominant over +1.5 eV, which are related to the d_{z^2} orbital of the Gd atom. Figure 4(a) shows that the Y site is affected by the d_{z^2} orbital because it is directly above the upper Gd atom of the top layer.

Then, we performed the STS simulation to understand the surface properties of the Gd_2C bilayer more deeply by converting the DOS plot in Figs. 5(a) and 5(b) into a 2D map. In the STS simulation, we used an energy range of 0.1 eV for the integration. As shown in Fig. 5(c), we obtained STS images for the peaks at −0.9, −0.4, +0.7, and +0.8 eV, indicated by arrows in Fig. 5(a). Indeed, the STS images obtained using a linear scale are foglike images because the heights of the peaks are similar in each energy range. The thick fog makes it impossible to distinguish between the Y, Y′, and Y″ sites. Therefore, we used an exponential scale for the STS simulation. As mentioned earlier, the peaks are more prominent in the bilayer (and trilayer) than in the monolayer.

Figure 5(c) shows that the bright spots in the 2D STS map exhibit a hexagonal lattice pattern. The STS images show that the energies for the spots are −0.9, −0.4, and +0.8 eV at Y′, which are in excellent agreement with the DOS peaks in Fig. 5(a). The bright spot of the Y′ site originates from the 5d orbitals in the Gd atom, and we confirm that the d_{xz} and d_{yz} orbitals of the Gd atom are associated with the Y′ site. In contrast, the Y site, which is located above the Gd atom, is brighter than the Y′ and Y″ sites at +0.7 eV.

Another exciting finding is that the 2D STS maps have hazy images at −0.9 and +0.8 eV. The energies are related to the bands of the IAE states in the Gd_2C bilayer band structure, as shown in Fig. 2(b). Around the K point, the IAE bands are almost flat near −0.9 and +0.8 eV, and the foglike image appearing at the surface is due to the SAEs. Because the symmetry is broken and the surface is exposed, SAEs cannot be precisely the same as those of the IAEs.

TABLE V. Calculated Fermi velocities for the IAE states of the bilayer, trilayer, tetralayer, and pentalayer. The unit is in 10^5 m/s.

Bilayer	Trilayer	Tetralayer	Pentalayer
3.956	4.385	4.445	4.303
	3.344	3.898	4.167
		3.603	4.088
			3.547

However, they are almost at the same energy level. We also present the STM images in Appendix C. The applied bias voltages were ±2.0 and ±1.0 V. The STM images exhibited hexagonal (triangular) lattice patterns at bias voltages of −2.0 and −1.0 V (+1.0 and +2.0 V). These images are also blurry as if the electron layer on the surface also causes fog.

IV. CONCLUSION

In summary, we studied the electronic properties of few-layer Gd_2C structures using first-principles calculations. To understand the relationship between the surface of the electride and the IAE states, which cannot be studied in bulk, we performed electronic structure calculations. We also investigated the effect of the external electric field on the few-layer Gd_2C. The work function of Gd_2C was found to be approximately 3.35 eV. We also found that the electronic bands of the IAE were in the conduction band. For spin-down electrons, one IAE band passes the Fermi level, contributing to the spin transport. Even if external molecules or ions stick to the surface of the electride, such external adsorbates cannot affect electron transport in the interlayer region. Finally, we performed STM and STS simulations. In the 2D STS map, blurry images appear at −0.9 eV and +0.8 eV which are created by an electron layer spreading on the surface. It behaves like a 2D electron gas (2DEG) appearing in a transistor. If more electrons are extracted from the top layer by applying a uniform electric field or gating from the outside, the density of the 2DEG can be controlled, and various exciting quantum transport studies can be conducted. Because Gd_2C shows the anomalous Hall effect [21], the 2DEG of the surface could also show stunning results for the Hall effect. As a future study, we will investigate how intrinsic and extrinsic defects in few-layer electrides affect SAE and IAE states, which may influence the transport of charge or spin.

ACKNOWLEDGMENTS

J.C. and G.K. acknowledge the Basic Science Research Program's financial support (Grant Nos. NRF-2019R1F1A1058177 and NRF-2020R1A6A1A03043435) through the National Research Foundation of Korea (NRF) funded by the Government of Korea. This work was also supported by the faculty research fund of Sejong University in 2019 (Grant No. 20190467).

APPENDIX A

The band structures of the model systems are shown in Fig. 6. The top and bottom panels show the band structures of the spin-up and spin-down electrons, respectively. In the spin-up electron band structure, the IAE band does not reach the Fermi level; however the IAE band passes the Fermi level for the spin-down band. Clearly, the monolayer has no IAE band in the band structure of the spin-down electrons. The Fermi velocity of the electron in the IAE band passing through the Fermi level in the circled region was 4.0×10^5 m/s. When the number of layers increases, the IAE bands in the conduction band interact with one another, resulting in a downshift of the IAE bands to the Fermi level.

APPENDIX B

We present the DOS plot of the difference between the systems with and without an electric field on the bilayer in Fig. 7. The red and blue dotted lines indicate the applied electric field case (0.1 V/Å and 0.4 V/Å). As shown in Fig. 4(b), the electronic density difference is small for the 0.1 V/Å case; thus, we present the magnified DOS plot in the lower panel of Fig. 7. The black rectangle in the upper panel denotes the range of the magnified DOS in the lower panel. From the enlarged version of the DOS plot, we identify that the electric field effects appear at the SAE sites (Y, Y′, and Y″), whereas they do not appear at the X and X′ sites. The DOS peaks of the SAE sites are downshifted because the

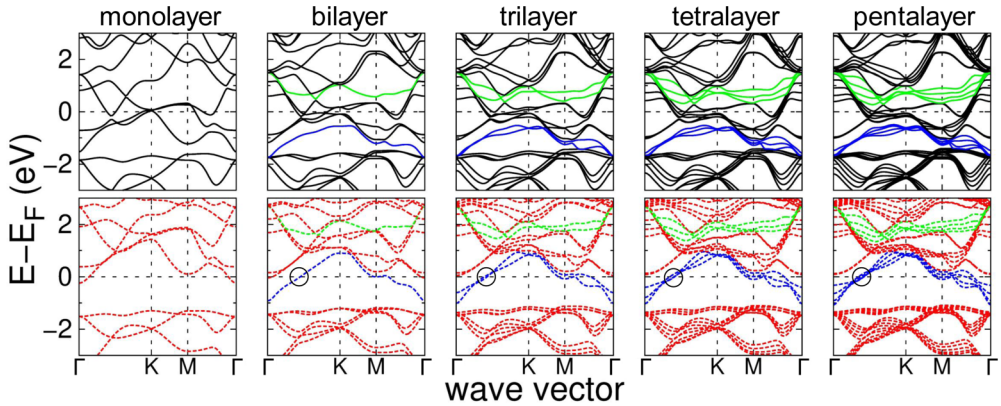

FIG. 6. Band structures of few-layer Gd_2C. Solid lines indicate spin-up states in the upper panel, and dashed lines indicate spin-down states in the lower panel. The bands marked with blue and green lines for spin-up and spin-down electrons represent IAE states, respectively.

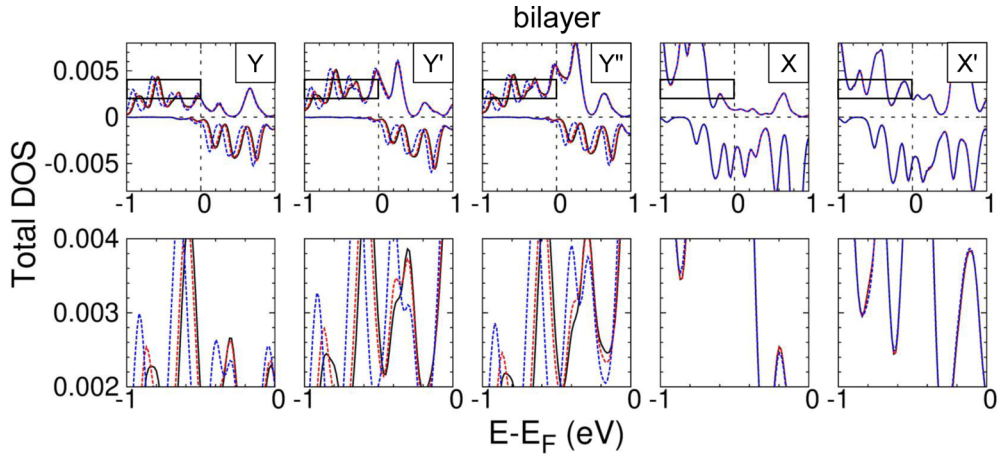

FIG. 7. DOS plot of the difference between the presence and absence of an electric field in the bilayer region. The solid black line represents the DOS for the absence of an electric field, and the dashed lines (red and blue) correspond to the presence of an electric field (0.1 V/Å and 0.4 V/Å). The DOS plot inside the black rectangle in the upper panel is enlarged and shown in the lower panel. The magnified DOS clearly shows the differences in the sites on the surface (Y, Y′, and Y″), whereas the differences are not revealed at the sites in the interlayer regions (X and X′).

number of electrons increases with the electric field. However, even when the external electric field changes, the DOS peaks at the X and X′ sites do not change much. Consequently, we confirmed the screening effect of Gd_2C and the electric field effect at the surface.

APPENDIX C

We performed STM simulations using the Tersoff-Hamann theory [45] and present the computed STM images in Fig. 8. We obtained STM images using a linear scale, although the images were blurry. The STM images exhibit hexagonal (triangular) patterns at the bias voltages of −2.0 and −1.0 V (+1.0 and +2.0 V). The STM images were related to the electron densities above the surface. In the energy ranges below the Fermi level, Y′ and Y″ sites were brighter in DOS than at the Y site, and the decomposed DOS of the Gd atom of the top layer showed that the d_{z^2} orbital is not dominant in this energy range. Therefore, the Y′ and Y″ sites form a hexagonal pattern at a bias voltage of −1.0 V.

Moreover, the STM images at the +1 V and +2 V bias voltages show a triangular pattern. Between −2 and +2 eV, the Y″ site has higher DOS peaks than the Y and Y′ sites, and the bright spots originate from the Y″ sites. The orbital decomposed DOS of the Gd atom, d_{z^2} orbital, is dominant in the energy range over +2 eV. Therefore, the Y site, which is the most affected by the d_{z^2} orbital, is not visible as a bright spot at the bias voltages of +1 and +2 V. The Y site has prominent DOS peaks at 3 eV or higher. If one obtains an STM image at 3 eV or higher, the Y site appears bright. In 2D space, the Y site corresponds to the Gd atom site on the surface.

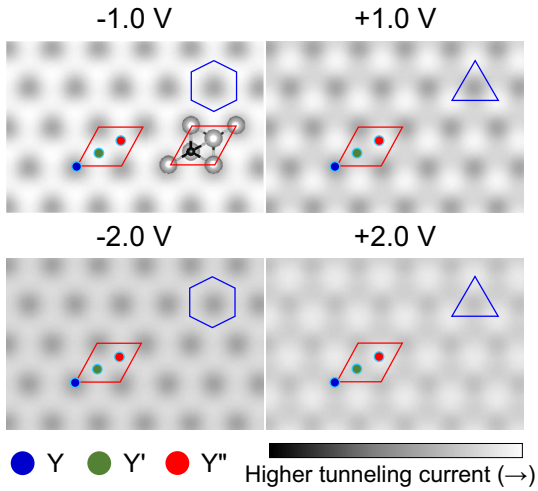

FIG. 8. STM images of the bilayer in the constant-height (2 Å) mode for each energy range. The red rhombus represents the unit cell of Gd_2C. Triangular patterns appear in the STM images at some energies, and honeycomb patterns appear at other energies.

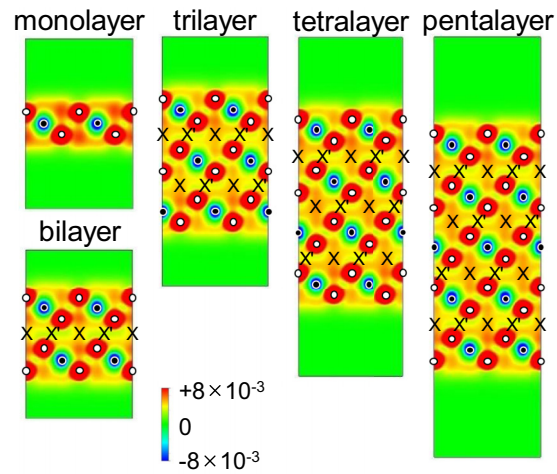

FIG. 9. The spin density plots of the Gd_2C ultrathin structures (from the monolayer to the pentalayer).

APPENDIX D

We show the electron spin density plots of the few-layered Gd_2C structures in Fig. 9. As mentioned earlier, the atomic spin magnetic moment of each Gd atom in Gd_2C is $\approx 7.3\ \mu_B$, and the highest spin density is shown in the Gd atom sites. Interestingly, the majority spin density appears in the interlayer space, which is consistent with a previous report on bulk Gd_2C [18].

[1] J. L. Dye, M. J. Wagner, G. Overney, R. H. Huang, T. F. Nagy, and D. Tománek, Cavities and channels in electrides, J. Am. Chem. Soc. **118**, 7329 (1996).

[2] J. L. Dye, Electrons as anions, Science **301**, 607 (2003).

[3] J. L. Dye, Electrides: Ionic salts with electrons as the anions, Science **247**, 663 (1990).

[4] J. L. Dye, Electrides: Early examples of quantum confinement, Acc. Chem. Res. **42**, 1564 (2009).

[5] T. Tada, S. Takemoto, S. Matsuishi, and H. Hosono, High-throughput *ab initio* screening for two-dimensional electride materials, Inorg. Chem. **53**, 10347 (2014).

[6] K. Lee, S. W. Kim, Y. Toda, S. Matsuishi, and H. Hosono, Dicalcium nitride as a two-dimensional electride with an anionic electron layer, Nature (London) **494**, 336 (2013).

[7] J. Park, K. Lee, S. Y. Lee, C. N. Nandadasa, S. Kim, K. H. Lee, Y. H. Lee, H. Hosono, S.-G. Kim, and S. W. Kim, Strong localization of anionic electrons at interlayer for electrical and magnetic anisotropy in two-dimensional Y_2C Electride, J. Am. Chem. Soc. **139**, 615 (2017).

[8] H. Huang, K.-H. Jin, S. Zhang, and F. Liu, Topological electride Y_2C, Nano Lett. **18**, 1972 (2018).

[9] M. Hirayama, S. Matsuishi, H. Hosono, and S. Murakami, Electrides as a New Platform of Topological Materials, Phys. Rev. X **8**, 031067 (2018).

[10] S. Matsuishi, Y. Toda, M. Miyakawa, K. Hayashi, T. Kamiya, M. Hirano, I. Tanaka, and H. Hosono, High-density electron anions in a nanoporous single crystal: $[Ca_{24}Al_{28}O_{64}]^{4+}(4e^-)$, Science **301**, 626 (2003).

[11] S. W. Kim, K. Hayashi, M. Hirano, H. Hosono, and I. Tanaka, Electron carrier generation in a refractory oxide $12CaO \cdot 7Al_2O_3$ by heating in reducing atmosphere: Conversion from an insulator to a persistent conductor, J. Am. Ceram. Soc. **89**, 3294 (2006).

[12] S. W. Kim, S. Matsuishi, T. Nomura, Y. Kubota, M. Takata, K. Hayashi, T. Kamiya, M. Hirano, and H. Hosono, Metallic state in a lime-alumina compound with nanoporous structure, Nano Lett. **7**, 1138 (2007).

[13] M. Miyakawa, S. W. Kim, M. Hirano, Y. Kohama, H. Kawaji, T. Atake, H. Ikegami, K. Kono, and H. Hosono, Superconductivity in an inorganic electride $12CaO \cdot 7Al_2O_3 : e^-$, J. Am. Chem. Soc. **129**, 7270 (2007).

[14] H. Hosono, S. W. Kim, S. Matsuishi, S. Tanaka, A. Miyake, T. Kagayama, and K. Shimizu, Superconductivity in room-temperature stable electride and high-pressure phases of alkali metals, Philos. Trans. R. Soc. A **373**, 20140450 (2015).

[15] S. W. Kim, Y. Toda, K. Hayashi, M. Hirano, and H. Hosono, Synthesis of a room temperature stable $12CaO \cdot 7Al_2O_3$ electride from the melt and its application as an electron field emitter, Chem. Mater. **18**, 1938 (2006).

[16] M. Kitano, Y. Inoue, Y. Yamazaki, F. Hayashi, S. Kanbara, S. Matsuishi, T. Yokoyama, S. W. Kim, M. Hara, and H. Hosono, Ammonia synthesis using a stable electride as an electron donor and reversible hydrogen store, Nat. Chem. **4**, 934 (2012).

[17] X. Zhang, Z. Xiao, H. Lei, Y. Toda, S. Matsuishi, T. Kamiya, S. Ueda, and H. Hosono, Two-dimensional transition-metal electride Y_2C, Chem. Mater. **26**, 6638 (2014).

[18] S. Y. Lee, J.-Y. Hwang, J. Park, C. N. Nandadasa, Y. Kim, J. Bang, K. Lee, K. H. Lee, Y. Zhang, Y. Ma, H. Hosono, Y. H. Lee, S.-G. Kim, and S. W. Kim, Ferromagnetic quasi-atomic electrons in two-dimensional electride, Nat. Commun. **11**, 1526 (2020).

[19] Y. Zhang, H. Wang, Y. Wang, L. Zhang, and Y. Ma, Computer-Assisted Inverse Design of Inorganic Electrides, Phys. Rev. X **7**, 011017 (2017).

[20] Y. Mudryk, Durga Paudyal, V. K. Pecharsky, and K. A. Gschneidner, Magnetic properties of Gd_2C: Experiment and first principles calculations, J. Appl. Phys. **109**, 07A924 (2011).

[21] S. Liu, C. Wang, L. Liu, J.-H. Choi, H.-J. Kim, Y. Jia, C. H. Park, and J.-H. Cho, Ferromagnetic Weyl Fermions in Two-Dimensional Layered Electride Gd_2C, Phys. Rev. Lett. **125**, 187203 (2020).

[22] S. Zhao, Z. Li, and J. Yang, Obtaining two-dimensional electron gas in free space without resorting to electron doping: An electride based design, J. Am. Chem. Soc. **136**, 13313 (2014).

[23] J. N. Coleman, Liquid exfoliation of defect-free graphene, Acc. Chem. Res. **46**, 14 (2013).

[24] D. L. Druffel, K. L. Kuntz, A. H. Woomer, F. M. Alcorn, J. Hu, C. L. Donley, and S. C. Warren, Experimental demonstration of an electride as a 2D material, J. Am. Chem. Soc. **138**, 16089 (2016).

[25] Y. Oh, J. Lee, J. Park, H. Kwon, I. Jeon, Kim S. W., G. Kim, S. Park, and S. W. Hwang, Electric field effect on the electronic structure of 2D Y_2C electride, 2D Mater. **5**, 035005 (2018).

[26] S. Kim, S. Song, J. Park, H. S. Yu, S. Cho, D. Kim, J. Baik, D.-H. Choe, K. J. Chang, Y. H. Lee, S. W. Kim, and H. Yang, Long-range lattice engineering of MoTe2 by a 2D electride, Nano Lett. **17**, 3363 (2017).

[27] B. Partoens and F. M. Peeters, From graphene to graphite: Electronic structure around the *k* point, Phys. Rev. B **74**, 075404 (2006).

[28] D. Wickramaratne, F. Zahid, and R. K. Lake, Electronic and thermoelectric properties of few-layer transition metal dichalcogenides, J. Chem. Phys. **140**, 124710 (2014).

[29] G. Kresse and J. Hafner, *Ab initio* molecular dynamics for liquid metals, Phys. Rev. B **47**, 558 (1993).

[30] G. Kresse and J. Furthmüller, Efficient iterative schemes for *ab initio* total-energy calculations using a plane-wave basis set, Phys. Rev. B **54**, 11169 (1996).

[31] G. Kresse and D. Joubert, From ultrasoft pseudopotentials to the projector augmented-wave method, Phys. Rev. B **59**, 1758 (1999).

[32] D. Hobbs, G. Kresse, and J. Hafner, Fully unconstrained noncollinear magnetism within the projector augmented-wave method, Phys. Rev. B **62**, 11556 (2000).

[33] J. P. Perdew, K. Burke, and M. Ernzerhof, Generalized Gradient Approximation Made Simple, Phys. Rev. Lett. **77**, 3865 (1996).

[34] S. L. Dudarev, G. A. Botton, S. Y. Savrasov, C. J. Humphreys, and A. P. Sutton, Electron-energy-loss spectra and the structural stability of nickel oxide: An LSDA+U study, Phys. Rev. B **57**, 1505 (1998).

[35] B. N. Harmon, V. P. Antropov, A. I. Liechtenstein, I. V. Solovyev, and V. I. Anisimov, Calculation of magneto-optical properties for 4f systems: LSDA+Hubbard U results, J. Phys. Chem. Solids **56**, 1521 (1995).

[36] V. I. Anisimov, F. Aryasetiawan, and A. I. Lichtenstein, First-principles calculations of the electronic structure and spectra of strongly correlated systems: The LDA+U method, J. Phys.: Condens. Matter **9**, 767 (1997).

[37] S. Abdelouahed, N. Baadji, and M. Alouani, Electronic structure and x-ray magnetic circular dichroism of gadolinium beyond the local spin density approximation, Phys. Rev. B **75**, 094428 (2007).

[38] T. Inoshita, S. Jeong, N. Hamada, and H. Hosono, Exploration for Two-Dimensional Electrides via Database Screening and *Ab Initio* Calculation, Phys. Rev. X **4**, 031023 (2014).

[39] S. Grimme, J. Antony, S. Ehrlich, and H. Krieg, A consistent and accurate *ab initio* parametrization of density functional dispersion correction (DFT-D) for the 94 elements H-Pu, J. Chem. Phys. **132**, 154104 (2010).

[40] J. O. Dimmock and A. J. Freeman, Band Structure and Magnetism of Gadolinium Metal, Phys. Rev. Lett. **13**, 750 (1964).

[41] H. E. Nigh, S. Legvold, and F. H. Spedding, Magnetization and electrical resistivity of gadolinium single crystals, Phys. Rev. **132**, 1092 (1963).

[42] L. W. Roeland, G. J. Cock, F. A. Muller, A. C. Moleman, K. A. McEwen, R. G. Jordan, and D. W. Jones, Conduction electron polarization of gadolinium metal, J. Phys. F **5**, L233 (1975).

[43] A. Sonntag, J. Hermenau, A. Schlenhoff, J. Friedlein, S. Krause, and R. Wiesendanger, Electric-Field-Induced Magnetic Anisotropy in a Nanomagnet Investigated on the Atomic Scale, Phys. Rev. Lett. **112**, 017204 (2014).

[44] J. Méndez, J. Gómez-Herrero, J. I. Pascual, J. J. Sáenz, J. M. Soler, and A. M. Baró, Diffusion of atoms on Au(111) by the electric field gradient in scanning tunneling microscopy, J. Vac. Sci. Technol. B **14**, 1145 (1996).

[45] J. Tersoff and D. R. Hamann, Theory of the scanning tunneling microscope, Phys. Rev. B **31**, 805 (1985).